Applied Physics Letters

Thermal-induced irreversible straining of ultrathin boron nitride nanosheets

Cite as: Appl. Phys. Lett. **114**, 051901 (2019); https://doi.org/10.1063/1.5083960
Submitted: 02 December 2018 . Accepted: 16 January 2019 . Published Online: 04 February 2019

Wenyang Qu, Feilin Gou, and Changhong Ke

Applied Physics Letters ARTICLE scitation.org/journal/apl

Thermal-induced irreversible straining of ultrathin boron nitride nanosheets

Cite as: Appl. Phys. Lett. **114**, 051901 (2019); doi: 10.1063/1.5083960
Submitted: 2 December 2018 · Accepted: 16 January 2019 ·
Published Online: 4 February 2019

Wenyang Qu,[1] Feilin Gou,[1] and Changhong Ke[1,2,a)]

AFFILIATIONS

[1] Department of Mechanical Engineering, State University of New York at Binghamton, Binghamton, New York 13902, USA
[2] Materials Science and Engineering Program, State University of New York at Binghamton, Binghamton, New York 13902, USA

[a)]Author to whom correspondence should be addressed: cke@binghamton.edu

ABSTRACT

We investigate the thermal-induced mechanical deformations in mono- and few-layer hexagonal boron nitride nanosheets (BNNSs) on flat silicon dioxide substrates by using atomic force microscopy and Raman spectroscopy techniques. The measurements reveal that the deformation of thin BNNS follows the reversible expansion/contraction of the substrate at relatively low temperatures. Irreversible deformations in BNNS are observed at elevated temperatures, which are attributed to interfacial sliding on the BNNS-substrate interface that is caused by the temperature-dependent thermal expansion mismatch of BN and substrate materials. Monolayer BNNS is found to possess the highest onset temperature of irreversible straining, which decreases with an increase in the BNNS thickness. The interfacial load transfer characteristics of the BNNS-substrate interface are quantitatively investigated using a micromechanics model. The analysis reveals that monolayer BNNS possesses a maximum interfacial shear strength of about 28.38 MPa on its binding interface with substrates at about 525 °C. The findings are useful to better understand the fundamental structural and mechanical properties of BNNS and in pursuit of its applications, in particular, those involved with high temperature processing and/or working environments.

Hexagonal boron nitride nanosheet (BNNS) reportedly possesses many extraordinary physical and chemical properties, such as a ultrahigh Young's modulus,[1–3] and superior thermal conductivity,[4] exceptional thermal and chemical stabilities,[5] and excellent electrically insulating characteristics.[6] BNNS has been investigated for a number of applications, including dielectric substrates in graphene nanoelectronics,[7] corrosion-protective coatings,[8] and mechanical and thermal fillers for polymeric,[9,10] metallic,[11] and ceramic[12] matrix nanocomposites. Many of these BNNS applications are involved with elevated temperature processing and/or working environments. Therefore, a complete understanding of the structural and physical properties of BNNS in high temperature environments is critical in pursuit of many of its practical applications. Due to its characteristics of a negative in-plane coefficient of thermal expansion (CTE),[13–15] thin BNNS tends to be stretched (compressed) when placed on substrates with positive CTEs at increasing (decreasing) temperatures. The deformation of BNNS results from the interfacial load transfer on the BNNS-substrate interface as a result of thermal expansion mismatches. While the thermal-induced expansion/contraction of substrates are typically reversible, irreversible deformation may occur in thin BNNS, which may lead to structural instabilities, such as wrinkles,[16] and thus have substantial impacts on the interface-relevant physical processes (e.g., load transfer and thermal transport) and overall applications and performances of BNNS-based devices and material systems. However, scientific understanding of the thermal-induced deformations in thin BNNS remains elusive.

Structurally, hexagonal BN is composed of partially ionic B-N bonds, and thus possesses an electrically corrugated landscape, which leads to stronger binding interactions or higher activation energies on interfaces with other material systems, such as polymers[17] and ceramics,[18,19] as compared with graphene that is composed of electrically neutral C-C bonds. A strong BNNS-substrate interface enables a relatively large thermal-induced reversible mechanical deformation in BNNS. In this paper, we investigate the thermal-induced mechanical deformations in monolayer (1L), bilayer (2L), and trilayer (3L) BNNS on flat silicon dioxide substrates by using atomic force microscopy (AFM) and Raman spectroscopy techniques. The measurements

reveal the reversible and irreversible mechanical deformations in thin BNNS at relatively low and high temperatures, respectively. Monolayer BNNS is found to possess the highest onset temperature of irreversible straining, which decreases with an increase in the BNNS thickness.

The BNNS flakes used in the study were prepared by mechanically exfoliating hexagonal BN platelets (Momentive, PT110).[18] The employed substrates were silicon wafers with a 90 nm oxide layer on top. The numbers of layers in BNNS flakes were identified by using AFM in conjunction with Raman microscopy. The AFM imaging measurements were performed by using a Park Systems XE-70 AFM that operates in the tapping mode at room temperature (about 23 °C) with silicon probes of less than 10 nm in nominal tip radius. The Raman measurements were performed by using a Renishaw InVia Raman microscope with a 532 nm wavelength excitation laser. The Raman spectra were collected by illumining the laser spot around the central region of BNNS domains to avoid or minimize the edge effects. Selected BNNS flakes with identified 1L-3L domains were subjected to repeated thermal heating/cooling treatments using a computer-controlled heating stage (Linkam TS 1500). BNNS samples were incrementally heated from room temperature to up to 550 °C in air at a rate of 5 °C/min. The heating was controlled to hold for 15 min at every 50 or 100 °C mark, and then the sample was cooled down to room temperature for AFM and *ex situ* Raman measurements. For *in situ* Raman measurements, BNNS samples were subjected to only the thermal heating process.

Figure 1(a) shows the AFM topography image of one as-prepared BNNS flake on a silicon oxide substrate that comprises multiple distinct thickness domains, while Fig. 1(b) shows one AFM image of the same sample after the controlled heating/cooling cycle that reached 550 °C. The topography profile of this flake along the marked A-A′ line, which is shown in Fig. 1(c), displays four steps with measured heights of about 0.62, 0.95, 0.97, and 1.31 nm, which are concluded to correspond to one 1L, two 2L, and one 3L domain, respectively. The identified numbers of layers in those BNNS domains are also confirmed through examination of their G band (E_{2g} mode) peak frequencies that are displayed in Figs. 2(a) and 2(b), and are consistent with prior reports.[18,20] A close examination of the AFM images shown in Figs. 1(a) and 1(b) reveals that the entire BN domains in this flake survived at 550 °C. The surface roughness of the examined BNNS domains is measured from the recorded AFM images and the results are displayed in Fig. 1(d), which shows that the surface roughness of the 1L domain is higher than those of the 2L and 3L domains at up to 300 °C. This observation is consistent with prior reports that the surface roughness of 2D thin films depends on the substrate roughness as well as their bending stiffness.[21–24] Thicker BNNS possesses a higher bending stiffness, which diminishes its deflection caused by the sample-substrate adhesion, and thus results in a smaller surface roughness. At up to 500 °C, the surface roughness of the 1L domain is found to remain in a narrow range of about 0.172–0.187 nm, which indicates its mechanical deformations during the repeated heating and cooling cycles were purely elastic and reversible. However, its surface roughness increases substantially at 550 °C to about 0.244 nm, which indicates that irreversible topographical corrugation occurred in the film. We believe that this irreversible deformation was caused by the compressive strain resulting from the CTE mismatch of h-BN and substrate materials. Similar changes in surface roughness are also observed for the 2L and 3L domains, but the prominent jumps occur at lower temperatures, i.e., 500 °C for the 2L and 400 °C for the 3L domains. Consistent measurements are shown on the two 2L domains. The results clearly reveal that thermal-induced irreversible deformations in BNNS depend on its thickness. 1L BNNS possesses the highest onset temperature for such irreversible straining, which decreases with an increase in the BNNS thickness.

We performed both *ex situ* and *in situ* Raman measurements to probe the mechanical deformations inside the BNNS films via monitoring the shift of their characteristic G band peak frequencies. Figure 2(a) shows the selected Raman spectra of the 1L domain in the BNNS flake shown in Fig. 1(a) that were recorded, *ex situ*, from room temperature to 550 °C. Its G band peak frequency, which is initially located at about 1370.17 cm^{-1} at room temperature, undergoes little change at up to 500 °C, which indicates purely elastic deformations in the BNNS during the repeated heating and cooling cycles. A prominent upshift to about 1371.39 cm^{-1} is observed when the temperature reaches 550 °C, which is also displayed in Fig. 2(b). The blueshift of about 1.2 cm^{-1} in wavenumber indicates that the BNNS was under a larger compression strain after this heating and cooling cycle as compared with its initial strain state at room temperature. Figure 2(b) shows similar G band peak frequency changes for the 2L and 3L domains, in which the jumps occurred at lower onset temperatures; i.e., 500 °C for 2L and 400 °C for 3L. By contrast, no prominent peak frequency change is observed on the spectra of bulk h-BN, as displayed in the inset plot in Fig. 2(b). It is noted that the observed Raman peak frequency changes in thin BNNS correspond well with the AFM measurement findings. The results reveal that thinner BNNS is able to follow the thermal expansion of the substrate at a greater temperature range. This can be explained by the fact that thinner BNNS has a lower tensile rigidity and is prone to stretch as compared to thicker ones. The results also suggest that sliding occurs on the BNNS-substrate interface at elevated temperatures and the critical temperature that enables interface sliding is higher for thinner sheets. For the tested BNNS domains shown in Fig. 1(a), the critical sliding onset temperature is considered to be 525 ± 25 °C for 1L, 450 ± 50 °C for 2L, and 350 ± 50 °C for 3L.

Figure 3(a) shows selected *in situ* Raman spectra of a 1L BNNS domain that was part of a flake as displayed in the inset AFM image. Its G band peak frequency is found to decrease from about 1370 cm^{-1} recorded at room temperature to about 1343 cm^{-1} at 550 °C, which indicates a redshift of 27 cm^{-1} in wavenumber for a temperature increase of about 527 °C. Figure 3(b) shows the *in situ* Raman G band peak frequency shift as a function of temperature for 1L-3L BNNS and bulk h-BN. The inset plot in Fig. 3(b) shows the dependence of the full width at half-maximum (FWHM) of the G band on temperature measured from the 1L spectra in Fig. 3(a), which displays a clear broadening trend between 300 and 550 °C.[25] The G band peak frequency

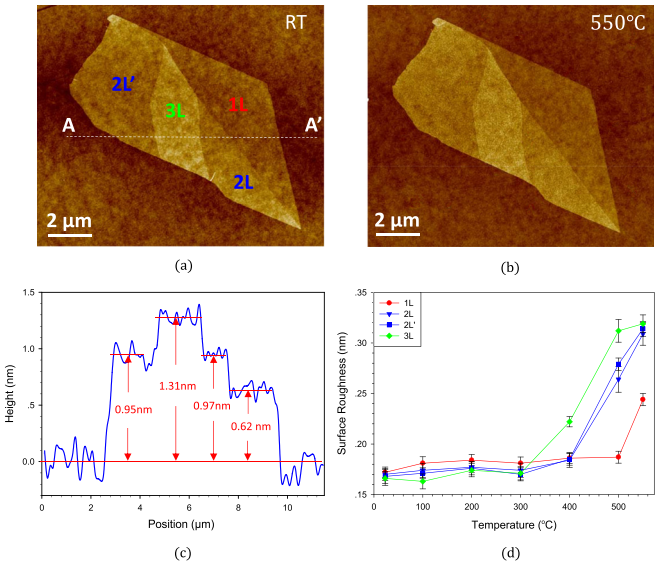

FIG. 1. (a) AFM image of one as-prepared BNNS flake consisting of one monolayer (marked as 1L), two bilayer (2L and 2L′), and one trilayer (3L) domains. (b) AFM image of the same flake in (a) after the heating/cooling cycle that reached 550 °C. (c) The topography profile along the marked line A-A′ in (a). (d) The surface roughness of each BNNS domain shown in (a) as a function of the maximum temperature in each heating/cooling cycle.

data of bulk h-BN can be well fitted by using a quadratic polynomial curve, while those of the 1L-3L BNNS follow linear trends. The observed downward shifts of the *in situ* Raman G band peak frequency in the 1L-3L BNNS are attributed to two effects: (i) *thermal effect*, which includes the thermal-induced expansion/contraction of BN sheets and phonon changes to BN bonds, both of which are independent of the sheet thickness;[15] (ii) *interface effect*, which represents the interfacial shearing-induced stretching of BN sheets as a result of the aforementioned CTE mismatch. The interface effect diminishes for thicker sheets and largely vanishes for bulk h-BN. Therefore, only thermal effect contributes to the frequency shift for bulk h-BN. The wavenumber difference in the *in situ* Raman peak frequency between thin BNNS and bulk h-BN recorded at room temperature is caused by the compressive pre-strain in thin BNNS that occurred during the sample preparation and transferring process[18] and is found to be about 4.6 cm^{-1} (1L), 3.8 cm^{-1}(2L), and 1.7 cm^{-1} (3L). With an increase in temperature, the wavenumber difference starts to decrease because the interface effect tends to stretch the sheet and offset the compressive pre-strain. Those crossover points between thin BNNS and h-BN curves indicate that mechanical strain in thin BNNS reached zero and the corresponding temperatures are found to be about 180 °C for 1L, 175 °C for 2L and 122 °C for 3L BNNS.

The G band peak frequency shift in 1L-3L BNNS caused by the interface effect alone can be assessed by subtracting the peak shift for bulk h-BN that is affected merely by the thermal effect from their respective *in situ* Raman spectra. Figure 3(c) shows the *in situ* G band peak frequency shift that is caused purely by the change of mechanical strain in BNNS. It is noted that the

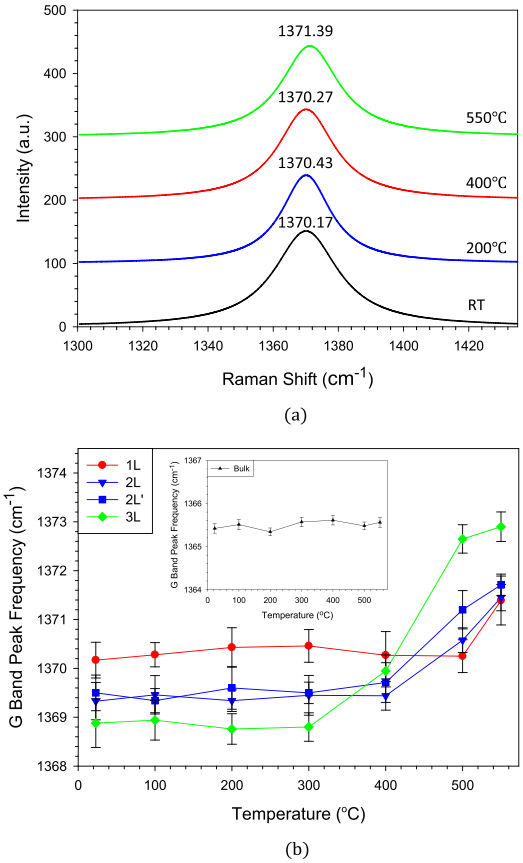

FIG. 2. *Ex situ* Raman spectroscopy measurements on the BNNS flake shown in Fig. 1(a). (a) Selected Raman spectra of the 1L BNNS domain. (b) The measured Raman G band peak frequency as a function of the maximum temperature in each heating/cooling cycle for all the BNNS domains. The inset is a control plot for bulk h-BN.

presented data are calculated with respect to the data recorded at room temperature. The change of mechanical strain in BNNS at a temperature t is calculated as $\Delta\varepsilon(t) = (CTE_{sub} - CTE_{BN}) \times (t - 23\,^{\circ}C)$, where $CTE_{sub} = 0.56 \times 10^{-6}/^{\circ}C$ is the CTE of silicon dioxide[26] and $CTE_{BN}(t) = (-2.3 \times 10^{-12}t^2 + 5.2 \times 10^{-9}t - 6.7 \times 10^{-6})/^{\circ}C$ is the CTE of h-BN.[15] The slopes of the three curves represent the sensitivity of the Raman peak frequency shift to mechanical strain and are calculated to be about 51.16 cm^{-1}/% (1L), 45.99 cm^{-1}/% (2L) and 43.68 cm^{-1}/% (3L). Consequently, the compressive pre-strains in thin BNNS at room temperature can be calculated based on their measured initial Raman peak frequency shifts with respect to h-BN and are found to be about −0.077% (1L), −0.075% (2L) and −0.041% (3L). The actual mechanical strain in BNNS up to the onset of interfacial sliding on the substrate, which is denoted as ε_0^{exp}, can be obtained by taking into account its initial pre-strain at room temperature and the results are displayed in Fig. 3(d). The maximum tensile strain in BNNS under reversible deformations is found to be about 0.164% ± 0.013% (1L), 0.132% ± 0.021% (2L), and 0.120% ± 0.021% (3L).

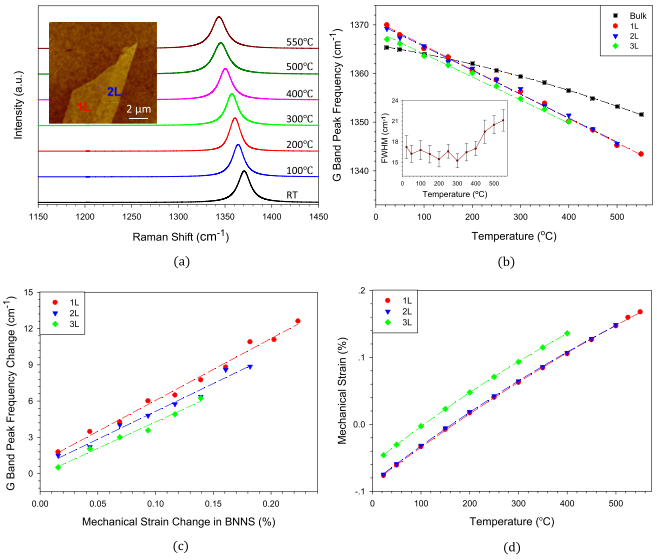

FIG. 3. *In situ* Raman spectroscopy measurements of BNNS flakes. (a) Selected Raman spectra recorded on one 1L BNNS domain. The employed BNNS flake, as displayed in the inset AFM image, consists of one 1L and one 2L domain. (b) The measured Raman G band peak frequency as a function of temperature for 1L to 3L BNNS. The 1L and 2L data were obtained from the two BNNS domains in the flake displayed in (a). The inset plot shows the dependence of the corresponding FWHM of the G band on temperature for the 1L domain. (c) G band peak frequency shift that is caused purely by the change of mechanical strain in BNNS. (d) The dependence of the mechanical strain in BNNS on temperature.

Finally, we investigate the interface load transfer characteristics between BNNS and the supporting substrate using a micromechanics model. The aforementioned data on the mechanical strain in BNNS due to thermal-induced expansion mismatch allow the simplification of the problem to the analysis of the mechanical deformation of a thin elastic sheet on a mechanically stretched elastic substrate. A one-dimensional representation of the model is illustrated in Fig. 4(a). In this model, the substrate deformation is assumed to occur only within a thin layer that is in a direct contact with the sheet that stays on top and is under pure shear deformations. The interfacial shear stress (IFSS) is applied to the sheet of length L via the shear deformation of the interfacial layer. The IFSS, τ_i, is in a linear relationship with the displacement of the sheet, $u(z)$, and is given as

$$\tau_i = \frac{G_m}{\delta} u(z), \tag{1}$$

where z is the coordinate axis with $z = 0$ at the sheet center; $u(z)$ is the displacement of the sheet; G_m is the shear modulus of the substrate material; and δ is the thickness of the interfacial layer. The equilibrium equation for the sheet is given as[27]

$$E^{2D} \frac{d^2 u(z)}{dz^2} = \frac{G_m}{\delta} u(z), \tag{2}$$

where E^{2D} is the 2D modulus of the sheet. The boundary conditions used in this model include the normal strain at the center of the sheet $(\varepsilon = du/dz)|_{z=0} = \varepsilon_0^{exp}$, while there is zero normal strain at its both ends (edges), i.e., $\varepsilon(z = \pm L/2) = 0$. The normal stress in the sheet is given as $\sigma(z) = \left(\int_z^{L/2} \tau_i dz\right)/(N \times t_{BN})$, in which N is the number of BN layers in the sheet and $t_{BN} = 0.34$ nm is the interlayer distance in h-BN. Equation (2) is solved with the following parameters: E^{2D} of BNNS is taken from prior experimental studies[3] as 289 N/m (for 1L), 590 N/m (for 2L), and 822 N/m (for 3L); $G_m = 30$ GPa for silicon dioxide.[28] By assuming a sheet length of 1.2 μm and considering $\delta = 23.9$ nm (a fitting value), Figs. 4(b) and 4(c) show the calculated respective IFSS and normal stress distribution profiles for 1L to 3L BNNS that correspond to their measured maximum reversible mechanical strains. The plots in Fig. 4(b) show that the IFSS possesses its maximum value at the sheet ends and decays rapidly toward the sheet center, which is a typical representation of the shear lag effect.[29] An effective interfacial load transfer occurs only along two relatively short lengths adjacent to both ends, the sum of which is found to be about 216 nm for 1L, 320 nm for 2L, and 400 nm for 3L BNNS. The strain in the central portion of the sheet tends to be uniform as long as its length is over the effective load transfer length. The maximum IFSS is found to be 28.38 ± 1.81 MPa for 1L BNNS, while 33.39 ± 5.27 MPa for 2L, and 36.47 ± 6.48 MPa for 3L BNNS. The results indicate that the thinner BNNS possesses a lower binding affinity with substrates, which can be ascribed to two factors. *First*, thicker BNNS has a stronger van der Waals interaction with the substrate than thinner ones. *Second*, prior studies show that an increasing temperature has a weakening effect on the van der Waals interactions.[30] The occurring temperature that corresponds to

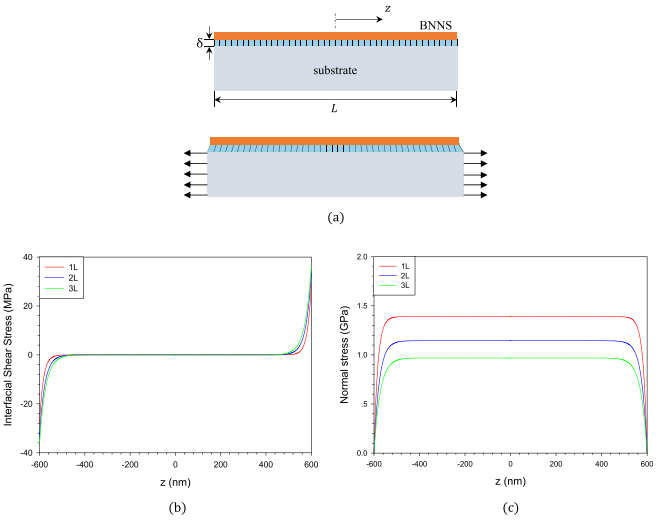

FIG. 4. Micromechanics modeling of the interfacial load transfer characteristics of a BNNS on a stretched substrate. (a) 1D illustration of the model (top: undeformed configuration; bottom: deformed configuration). The blue shaded region is the assumed interfacial layer with a thickness of δ that is under pure shear deformation. Vertical meshes are added to aid the visualization of its shear deformations. (b) and (c) The theoretically calculated interfacial shear stress (b) and normal stress (c) distribution profiles for 1L-3L BNNS. A sheet length of 1.2 μm is assumed in the calculation.

the calculated maximum IFSS is higher for thinner BNNS, which inevitably leads to a lower van der Waals interactions, and thus the binding affinity with the substrate. Therefore, the influence of temperature plays an important role in the proper interpretation of the calculated maximum IFSS results for thin BNNS. As displayed in Fig. 4(c), the calculated maximum normal stress in BNNS is located in its central portion and is found to be about 1.39 GPa (1L), 1.14 GPa (2L) and 0.97 GPa (3L). It is noted that our analysis shows that the value of the fitting parameter δ is dependent on the elastic properties of the substrate and tends to be smaller for substrate materials with lower Young's moduli.

In summary, the thermal-induced mechanical deformations in ultrathin BNNS on silicon oxide substrates are investigated. The measurements reveal that monolayer BNNS possesses the highest onset temperature of irreversible straining, which decreases with an increase in BNNS thickness. The dependence of the Raman peak frequency shift on the mechanical strain in BNNS is obtained. The study shows that thermal-induced deformations in 2D materials are useful in probing their interfacial binding interaction with other bulk materials. The findings are useful to better understand the fundamental structural and mechanical properties of BNNS and in pursuit of its applications, in particular those involved with high temperature processing and/or working environments.

This work was supported by the U.S. Air Force Office of Scientific Research-Low Density Materials program under Grant No. FA9550-15-1-0491 and by the National Science Foundation under Grant No. CMMI-1537333.

REFERENCES

[1]A. Bosak, J. Serrano, M. Krisch, K. Watanabe, T. Taniguchi, and H. Kanda, Phys. Rev. B **73**, 041402 (2006).
[2]L. Boldrin, F. Scarpa, R. Chowdhury, and S. Adhikari, Nanotechnology **22**, 505702 (2011).
[3]A. Falin, Q. Cai, E. J. G. Santos, D. Scullion, D. Qian, R. Zhang, Z. Yang, S. Huang, K. Watanabe, T. Taniguchi *et al.*, Nat. Commun. **8**, 15815 (2017).
[4]T. Ouyang, Y. Chen, Y. Xie, K. Yang, Z. Bao, and J. Zhong, Nanotechnology **21**, 245701 (2010).
[5]L. H. Li, J. Cervenka, K. Watanabe, T. Taniguchi, and Y. Chen, ACS Nano **8**, 1457 (2014).
[6]G. Cassabois, P. Valvin, and B. Gil, Nat. Photonics **10**, 262 (2016).
[7]C. R. Dean, A. F. Young, I. Meric, C. Lee, L. Wang, S. Sorgenfrei, K. Watanabe, T. Taniguchi, P. Kim, K. L. Shepard *et al.*, Nat. Nanotechnol. **5**, 722 (2010).
[8]W. Sun, L. Wang, T. Wu, Y. Pan, and G. Liu, J. Electrochem. Soc. **163**, C16 (2016).
[9]C. Zhi, Y. Bando, C. Tang, H. Kuwahara, and D. Golberg, Adv. Mater. **21**, 2889 (2009).
[10]M. S. R. N. Kiran, K. Raidongia, U. Ramamurty, and C. N. R. Rao, Scr. Mater. **64**, 592 (2011).
[11]S. Nam, K. Chang, W. Lee, M. J. Kim, J. Y. Hwang, and H. Choi, Sci. Rep. **8**, 1614 (2018).
[12]P. Tatarko, S. Grasso, H. Porwal, Z. Chlup, R. Saggar, I. Dlouhý, and M. J. Reece, J. Eur. Ceram. Soc. **34**, 3339 (2014).
[13]B. Yates, M. J. Overy, and O. Pirgon, Philos. Mag. **32**, 847–857 (1975).
[14]X. Z. Du, J. Li, J. Y. Lin, and H. X. Jiang, Appl. Phys. Lett. **111**, 132106 (2017).
[15]P. Anees, M. C. Valsakumar, and B. K. Panigrahi, Phys. Chem. Chem. Phys. **18**, 2672 (2016).
[16]C. K. Oliveira, E. F. A. Gomes, M. C. Prado, T. V. Alencar, R. Nascimento, L. M. Malard, R. J. C. Batista, A. B. de Oliveira, H. Chacham, A. M. de Paula *et al.*, Nano Res. **8**, 1680 (2015).
[17]X. Chen, L. Zhang, C. Park, C. C. Fay, X. Wang, and C. Ke, Appl. Phys. Lett. **107**, 253105 (2015).
[18]W. Qu, X. Chen, and C. Ke, Appl. Phys. Lett. **110**, 143110 (2017).
[19]C. Yi, S. Bagchi, F. Gou, C. M. Dmuchowski, C. Park, C. C. Fay, H. B. Chew, and C. Ke, Nanotechnology **30**, 025706 (2019).
[20]R. V. Gorbachev, I. Riaz, R. R. Nair, R. Jalil, L. Britnell, B. D. Belle, E. W. Hill, K. S. Novoselov, K. Watanabe, T. Taniguchi, A. K. Geim, and P. Blake, Small **7**, 465 (2011).
[21]X. Li, W. Cai, J. An, S. Kim, J. Nah, D. Yang, R. Piner, A. Velamakanni, I. Jung, E. Tutuc *et al.*, Science **324**, 1312 (2009).
[22]T. Li and Z. Zhang, J. Phys. D: Appl. Phys. **43**, 075303 (2010).
[23]C. Mattevi, H. Kim, and M. Chhowalla, J. Mater. Chem. **21**, 3324 (2011).
[24]W. Gao and R. Huang, J. Phys. D: Appl. Phys. **44**, 452001 (2011).
[25]R. J. Nemanich, S. A. Solin, and R. M. Martin, Phys. Rev. B **23**, 6348 (1981).
[26]B. El-Kareh, *Fundamentals of Semiconductor Processing Technology* (Springer, 1995).
[27]C. Yi, X. Chen, F. Gou, C. M. Dmuchowski, A. Sharma, C. Park, and C. Ke, Carbon **125**, 93 (2017).
[28]G. Carlotti, L. Doucet, and M. Dupeux, Thin Solid Films **296**, 102 (1997).
[29]X. Chen, M. Zheng, C. Park, and C. Ke, Small **9**, 3345 (2013).
[30]A. V. Pinon, M. Wierez-Kien, A. D. Craciun, N. Beyer, J. L. Gallani, and M. V. Rastei, Phys. Rev. B **93**, 035424 (2016).